Supporting Information

Europium-Functionalized Flexible Luminescent Zeolite-like Supramolecular Assembly for Ratiometric Anthrax Biomarker Determination

Kai Xing, Ruiqing Fan,* Shuang Gai, Xubin Zheng, Ping Wang, and Yulin Yang*

MIIT Key Laboratory of Critical Materials Technology for New Energy Conversion and Storage, School of Chemistry and Chemical Engineering, Harbin Institute of Technology, Harbin, Heilongjiang 150001, P. R. China

* Corresponding Author: Ruiqing Fan and Yulin Yang

E-mail: fanruiqing@hit.edu.cn and ylyang@hit.edu.cn

Contents

Section 1. Experimental Section S-3

Section 2. Structural Information for 1–3 ..... S-4

Section 3. General characterization S-12

Section 4. Photophysical studies of 1–3 ..... S-15

Section 5. Solvent dependent dynamic property S-16

Section 6. DPA detection of Eu^{3+}@3 composite S-18

Section 1. Experimental Section

Materials and Methods

All reagents were commercially available and used without further purification. FT-IR spectra were obtained from KBr pellets, using a Nicolet Avatar-360 Infrared spectrometer in the 4000–400 cm^{-1} region. Elemental analyses were performed on a Perkin-Elmer 240c element analyzer. Powder X-ray diffraction (PXRD) patterns were recorded in the 2θ range of 5–50° using Cu Kα radiation by Shimadzu XRD-6000 X-ray Diffractometer. The thermal analysis was performed on a ZRY-2P thermogravimetric analyzer from 25 to 750 °C with heating rate of 10 °C min^{-1} under a flow of air. Luminescence analysis and luminescence lifetimes were recorded on Edinburgh FLS920 luminescence spectrometer at 298 K. Elemental analyses for Cd and Eu were conducted using a Perkin-Elmer Model Optima 3300 DV ICP spectrometer. Density functional theory (DFT) calculations were conducted by using the B3LYP/lanl2dz basis set implemented in the Gaussian 09 package. XPS experiments were carried out on a RBD upgraded PHI-5000C ESCA system (Perkin Elmer) with Mg Kα radiation ($h\nu$ = 1253.6 eV).

Single-Crystal X-Ray Crystal Structure Determination

The X-ray diffraction data taken at room temperature for **1**–**3** were collected on a Rigaku R-AXIS RAPID IP diffractometer equipped with graphite-monochromated Mo Kα radiation (λ = 0. 71073 Å). The structures of **1**–**3** were solved by direct methods and refined on F^2 by the full-matrix least squares using the SHELXTL-97 crystallographic software.[1, 2] Anisotropic thermal parameters are refined to all of the non-hydrogen atoms. The hydrogen atoms were held in calculated ideal positions on carbon atoms and nitrogen atoms in ligands and that were directly included in the molecular formula on water molecules. The chemical formulas were determined by the combination of single crystal data, TGA results and elemental analysis. The CCDC 1937720, 1937721 and 1937722 contain the crystallographic data **1**–**3** of this paper. These data can be obtained free of charge at www.ccdc.cam.ac.uk/ deposit. Crystal structure data and details of the data collection and the structure refinement are listed as Table S1, selected bond lengths and bond angles of **1**–**3** are listed as Table S3-S5.

Section 2. Structural Information for 1–3

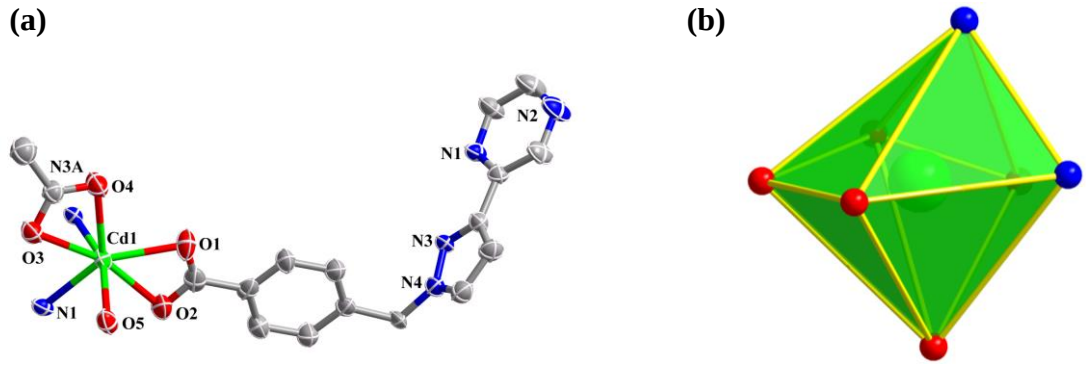

Figure S1. (a) The structural unit of **1** with labeling scheme and 50% thermal ellipsoids; (b) Polyhedral representation of the coordination sphere of the Cd^{2+} center in **1** (Hydrogen atoms are omitted for clarity).

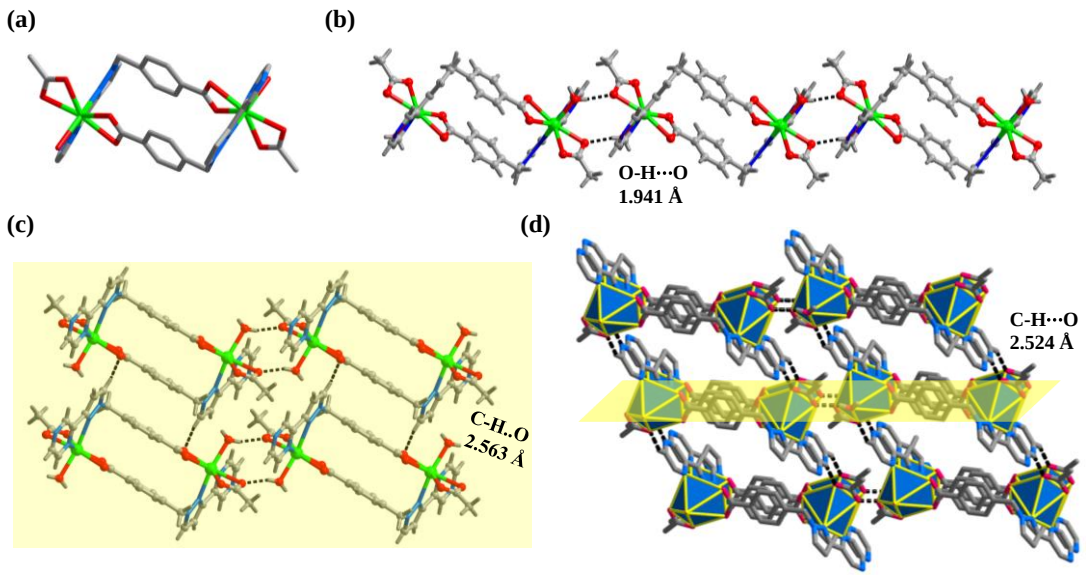

Figure S2. (a) The dimer structure in **1**; (b) Ball-and-stick representation of the 1D chain structure ; (c) The 2D layer structure in **1**; (d) 3D supramolecular structure of **1** (Hydrogen bonds are shown by black dash lines).

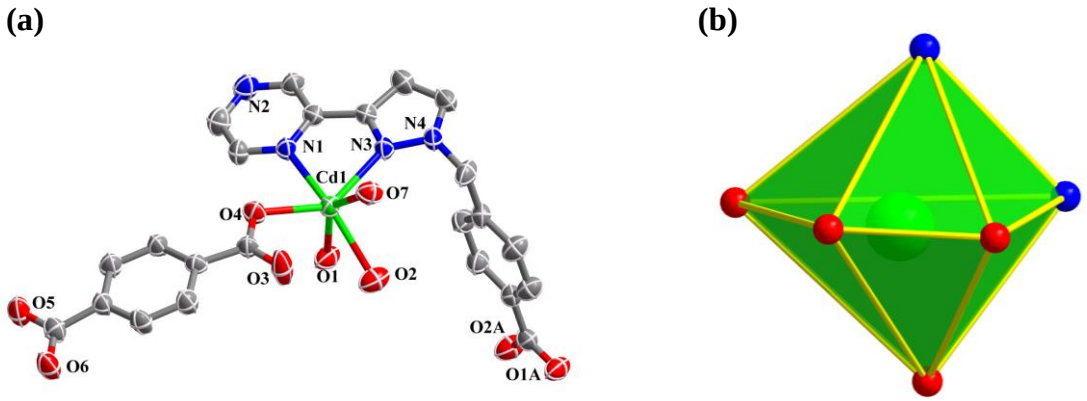

Figure S3. (a) The structural unit of **2** with labeling scheme and 50% thermal ellipsoids; (b) Polyhedral representation of the coordination sphere of the Cd^{2+} center in **2** (Free water molecules and hydrogen atoms are omitted for clarity).

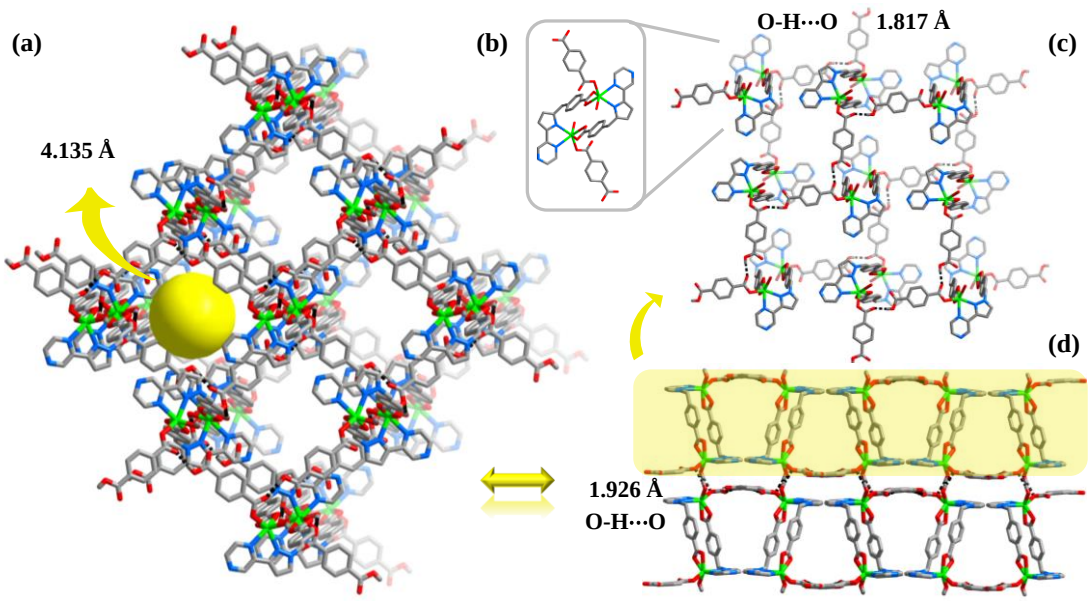

Figure S4. (a) 3D supramolecular structure with square window along (101) direction in **2**; (b)The dimer structure in **2**; (c) The 2D layer structure in **2**; (d) 3D supramolecular structure along *c* axis in **2** (Hydrogen bonds are shown by black dash lines).

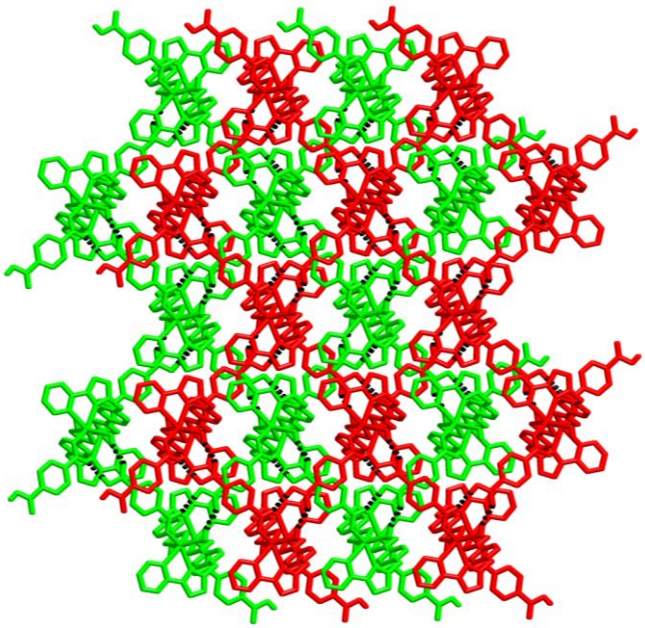

Figure S5. Stick representation of the 3D two-fold interpenetration structure of **2**.

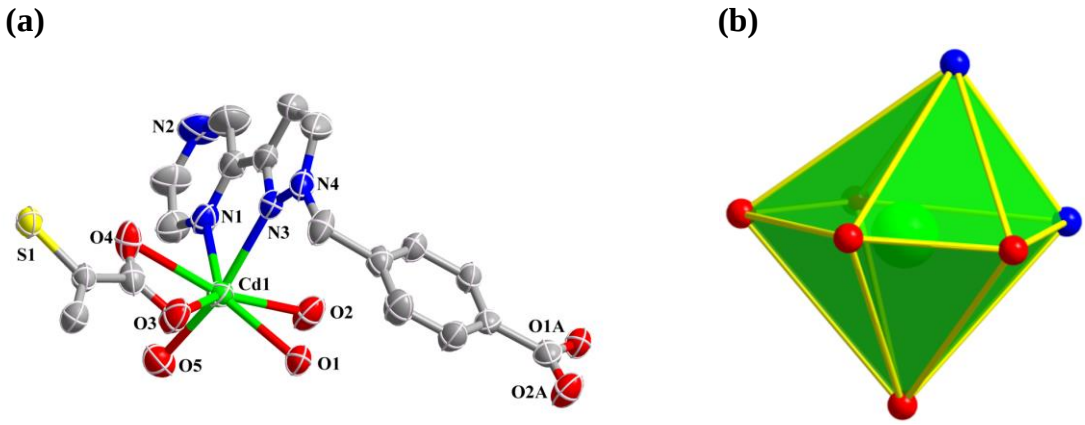

Figure S6. (a) The structural unit of **3** with labeling scheme and 50% thermal ellipsoids; (b) Polyhedral representation of the coordination sphere of the Cd^{2+} centre in **3** (Free water molecules and hydrogen atoms are omitted for clarity).

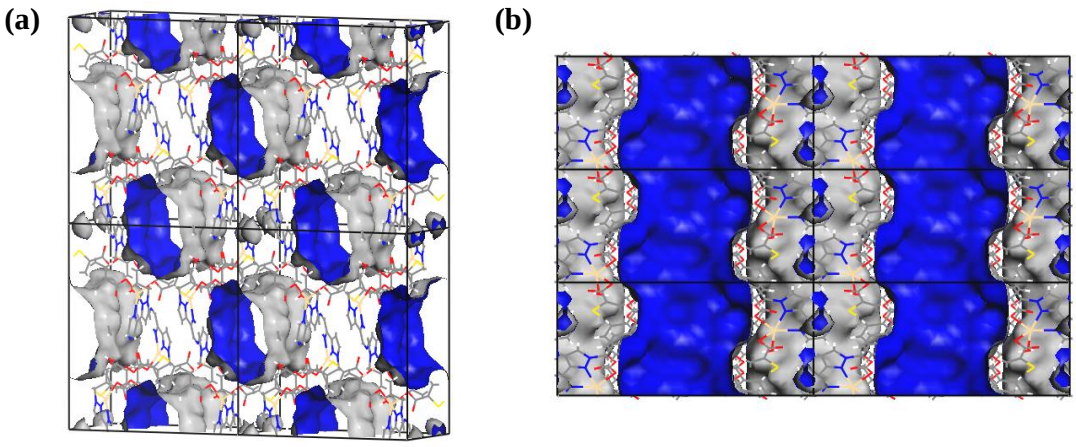

Figure S7. Solvent accessible void space along *a* (a) and *c*-axis (b) (gray: outer site of the pore and blue: inner site of the pore) of **3**, respectively.

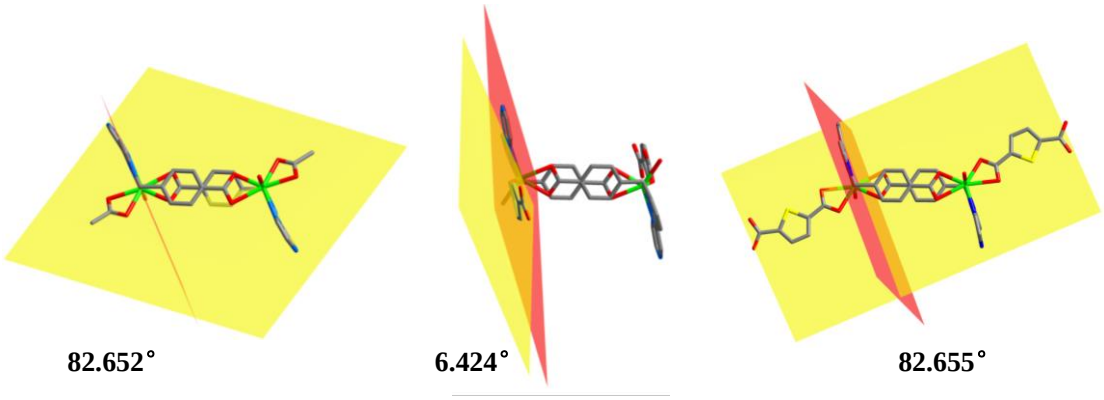

Figure S8. The dihedral angel between heterocyclic ring and auxiliary ligand in **1** (left), **2** (middle) and **3** (right) (hydrogen atoms are omitted for clarity).

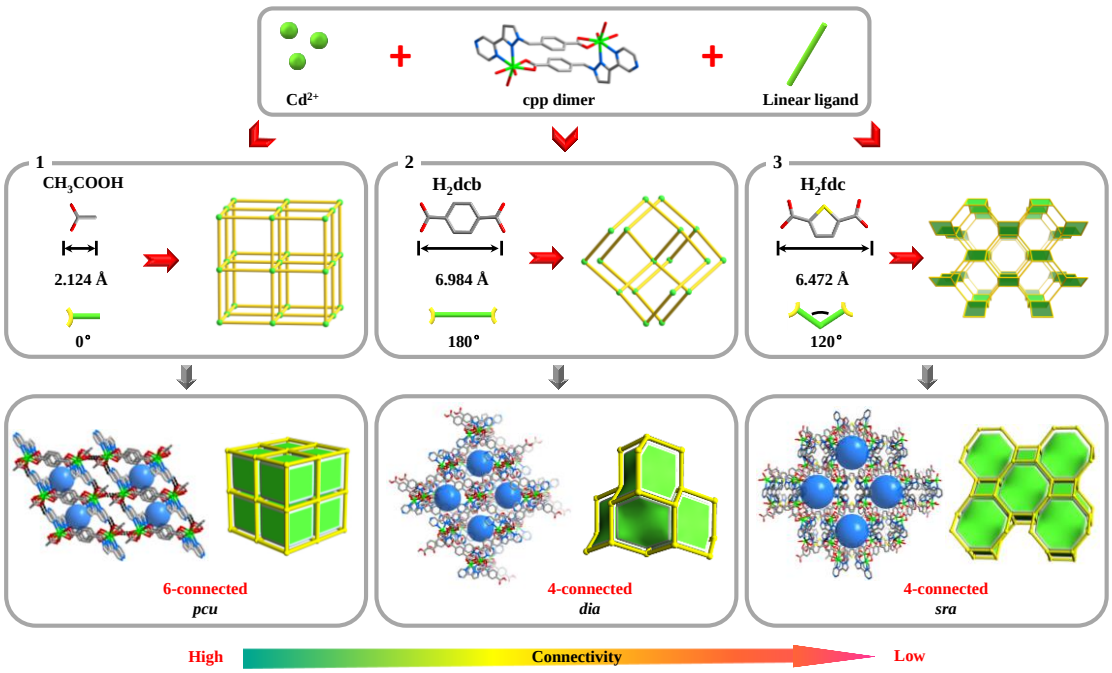

Figure S9. Topology transformation with decreased connectivity based on ***pcu*** MOA by controlling the bridging angle of ditopic ligand.

Table S1. Crystal data and structure refinement parameters of **1–3**.

Identification code	**1**	**2**	**3**
Empirical formula	$C_{34}H_{32}Cd_2N_8O_{10}$	$C_{46}H_{40}Cd_2N_8O_{16}$	$C_{36}H_{38}Cd_2N_8O_{15}S$
Formula mass	937.50	1185.66	1079.63
Crystal system	Triclinic	Monoclinic	Monoclinic
Space group	*P*1	$P2_1/n$	*C*2/c
a (Å)	7.9887(15)	9.178(3)	20.172(2)
b (Å)	8.5278(16)	19.687(7)	22.752(2)
c (Å)	15.021(3)	12.828(5)	10.0747(11)
α (˚)	97.619(2)	90	90
β (˚)	100.389(2)	100.207(4)	94.561(2)
γ (˚)	108.692(2)	90	90
V ($Å^3$)	933.3(3)	2281.0(14)	4609.2(8)
Z	1	2	4
D_c/(g · cm^{-3})	1.668	1.726	1.556
μ (Mo Kα)/mm^{-1}	1.206	1.016	1.039
F(000)	468	1192	2168
θ range (˚)	1.41 – 25.00	1.92 – 27.02	1.35 –25.00
Limiting indices	$-9 \le h \le 9$ $-10 \le k \le 10$ $-17 \le l \le 17$	$-11 \le h \le 11$ $-24 \le k \le 24$ $-14 \le l \le 15$	$-23 \le h \le 23$ $-27 \le k \le 27$ $-11 \le l \le 11$
Data/Restraints/Parameters	3286 / 0 / 234	4537 / 0 / 325	4055 / 0 / 281
GOF on F^2	1.092	1.036	1.110
Final *R* indices [$I > 2\sigma(I)$]			
R_1[a]	0.0363	0.0299	0.0495
wR_2[b]	0.0964	0.0786	0.1483
R indices (alldata)			
R_1	0.0438	0.0396	0.0846
wR_2	0.1067	0.0835	0.1730
CCDC	1937720	1937721	1937722

[a] $R_1 = \sum||F_o| - |F_c||/\sum|F_o|$; [b] $wR_2 = [\sum[w(F_o^2 - F_c^2)^2] / \sum[w(F_o^2)^2]]^{1/2}$.

Table S2. Hydrogen-bond (Å, deg) for **1-3**.

MOA	D-H⋯A	d(H..A)	<DHA	d(D..A)
1	O5-H5⋯O3	1.940	160.88	2.758
	C7-H7⋯O2	2.563	141.47	3.341
	C2-H2⋯O4	2.524	156.21	3.396
2	O5-H5A⋯O3	1.818	162.94	2.613
	O7-H7A⋯O4	1.926	169.86	2.767
3	C4-H4A⋯O4	2.448	177.28	3.375

Table S3. Selected bond distance (Å) and angles (˚) in **1**.

1					
Cd(1)-O(1)	2.281(3)	Cd(1)-O(5)	2.346(3)	Cd(1)-O(4)	2.384(3)
Cd(1)-N(3)#1	2.390(4)	Cd(1)-N(1)#1	2.396(4)	Cd(1)-O(3)	2.402(3)
Cd(1)-O(2)	2.448(4)				
O(1)-Cd(1)-O(5)	95.21(12)	O(1)-Cd(1)-O(4)	86.55(13)	O(5)-Cd(1)-O(4)	104.29(13)
O(1)-Cd(1)-N(3)#1	102.65(12)	O(5)-Cd(1)-N(3)#1	158.60(12)	O(4)-Cd(1)-N(3)#1	88.63(12)
O(1)-Cd(1)-N(1)#1	138.53(13)	O(5)-Cd(1)-N(1)#1	89.79(12)	O(4)-Cd(1)-N(1)#1	131.88(12)
N(3)#1-Cd(1)-N(1)#1	69.02(12)	O(1)-Cd(1)-O(3)	138.66(13)	O(5)-Cd(1)-O(3)	84.51(11)
O(4)-Cd(1)-O(3)	54.04(11)	N(3)#1-Cd(1)-O(3)	89.67(12)	N(1)#1-Cd(1)-O(3)	82.78(12)
O(5)-Cd(1)-O(2)	88.00(12)	O(4)-Cd(1)-O(2)	141.02(12)	N(3)#1-Cd(1)-O(2)	92.54(12)
N(1)#1-Cd(1)-O(2)	83.98(13)	O(3)-Cd(1)-O(2)	164.80(12)		

Symmetry transformations used to generate equivalent atoms:
#1 -x+1,-y,-z+1

Table S4. Selected bond distance (Å) and angles (˚) in **2**.

2					
Cd(1)-O(4)	2.252(2)	Cd(1)-O(2)	2.349(2)	Cd(1)-O(1)	2.336(3)
Cd(1)-O(7)	2.297(2)	Cd(1)-N(3)	2.357(2)	Cd(1)-N(1)	2.429(2)
O(4)-Cd(1)-O(7)	97.01(8)	O(4)-Cd(1)-O(2)	116.08(9)	O(4)-Cd(1)-N(3)	141.28(7)
O(4)-Cd(1)-O(1)	102.39(8)	O(7)-Cd(1)-O(2)	88.01(8)	O(7)-Cd(1)-N(3)	86.00(8)
O(7)-Cd(1)-O(1)	143.40(8)	O(1)-Cd(1)-O(2)	55.60(8)	O(1)-Cd(1)-N(3)	97.33(8)
O(2)-Cd(1)-N(3)	102.57(9)	O(1)-Cd(1)-N(1)	84.81(8)	O(7)-Cd(1)-N(1)	129.52(8)
O(4)-Cd(1)-N(1)	79.46(8)	O(2)-Cd(1)-N(1)	139.00(8)	N(3)-Cd(1)-N(1)	69.47(8)

Symmetry transformations used to generate equivalent atoms:
#1 -x+2,-y,-z+1

Table S5. Selected bond distance (Å) and angles (˚) in **3**.

		3			
Cd(1)-O(1)	2.293(5)	Cd(1)-N(1)	2.360(6)	Cd(1)-O(4)	2.539(5)
Cd(1)-O(5)	2.294(5)	Cd(1)-N(3)	2.362(6)	Cd(1)-O(2)	2.495(5)
Cd(1)-O(3)	2.328(5)				
O(1)-Cd(1)-O(5)	97.34(19)	O(1)-Cd(1)-N(1)	133.04(18)	O(1)-Cd(1)-N(3)	96.99(18)
O(1)-Cd(1)-O(3)	91.64(18)	O(5)-Cd(1)-N(1)	91.1(2)	O(5)-Cd(1)-N(3)	161.6(2)
O(5)-Cd(1)-O(3)	93.0(2)	O(3)-Cd(1)-N(1)	134.11(19)	O(3)-Cd(1)-N(3)	98.1(2)
N(1)-Cd(1)-N(3)	70.6(2)	O(3)-Cd(1)-O(2)	145.96(18)	O(1)-Cd(1)-O(4)	145.00(18)
O(1)-Cd(1)-O(2)	54.37(16)	N(1)-Cd(1)-O(2)	79.17(18)	O(5)-Cd(1)-O(4)	91.2(2)
O(5)-Cd(1)-O(2)	93.2(2)	N(3)-Cd(1)-O(2)	85.78(19)	O(3)-Cd(1)-O(4)	53.91(17)
N(1)-Cd(1)-O(4)	80.33(19)	N(3)-Cd(1)-O(4)	83.65(19)	O(2)-Cd(1)-O(4)	159.10(18)

Symmetry transformations used to generate equivalent atoms:
#1 -x,y,-z+5/2 #2 -x+1/2,-y+1/2,-z+1

Section 3. General characterization

IR spectra of 1–3

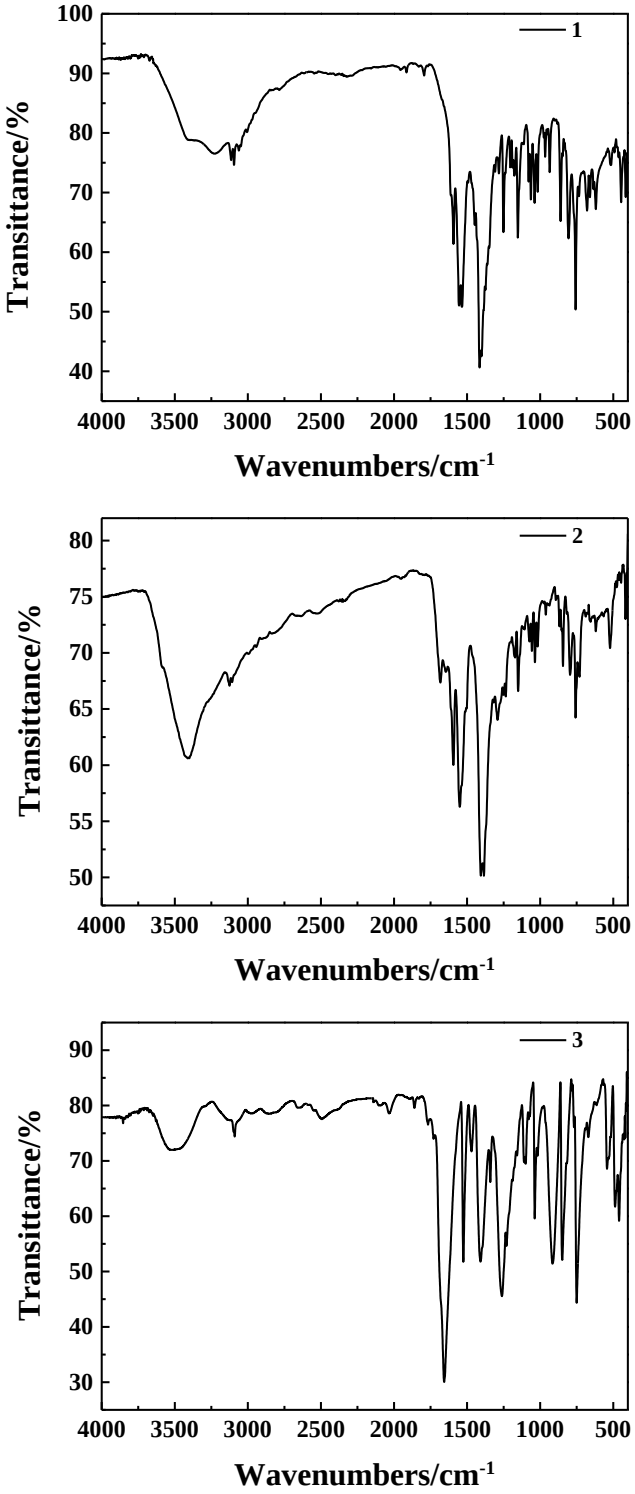

Figure S10. Infrared spectra of **1–3** recorded from a KBr pellet.

The PXDR patterns of 1–3

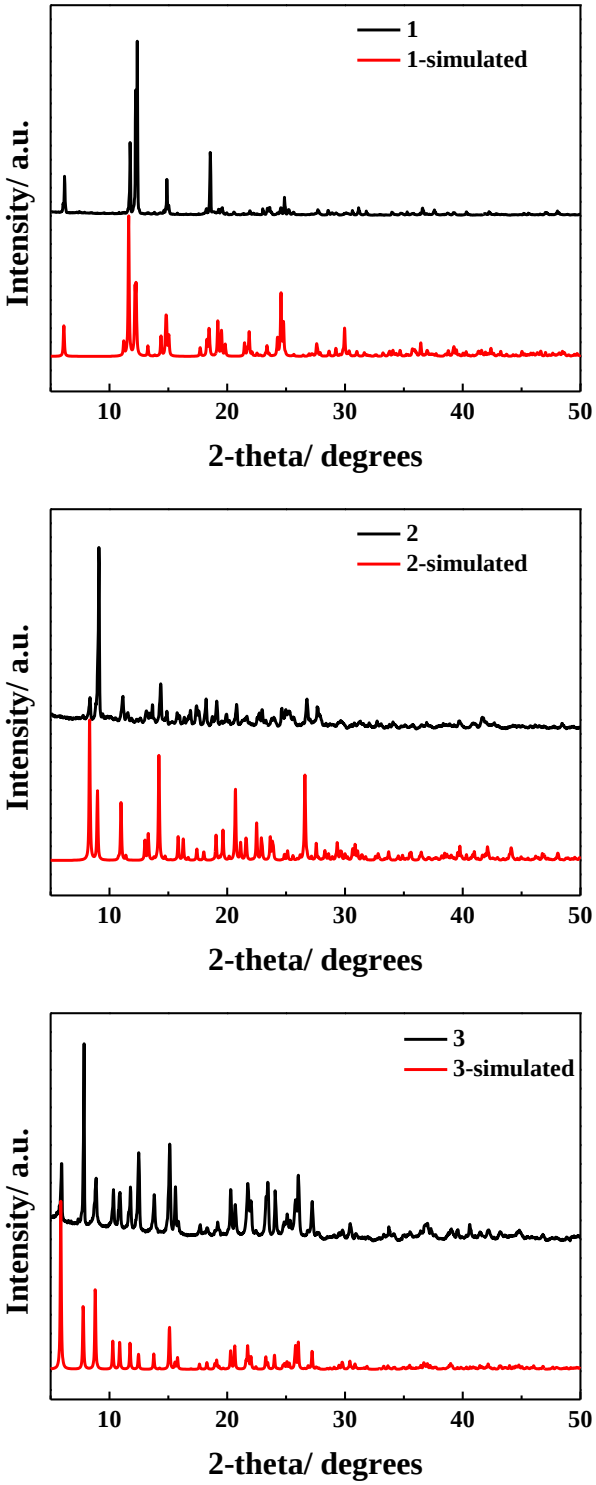

Figure S11. The PXRD contrast curves of **1–3** with the relevant simulated patterns.

The TGA for 1–3

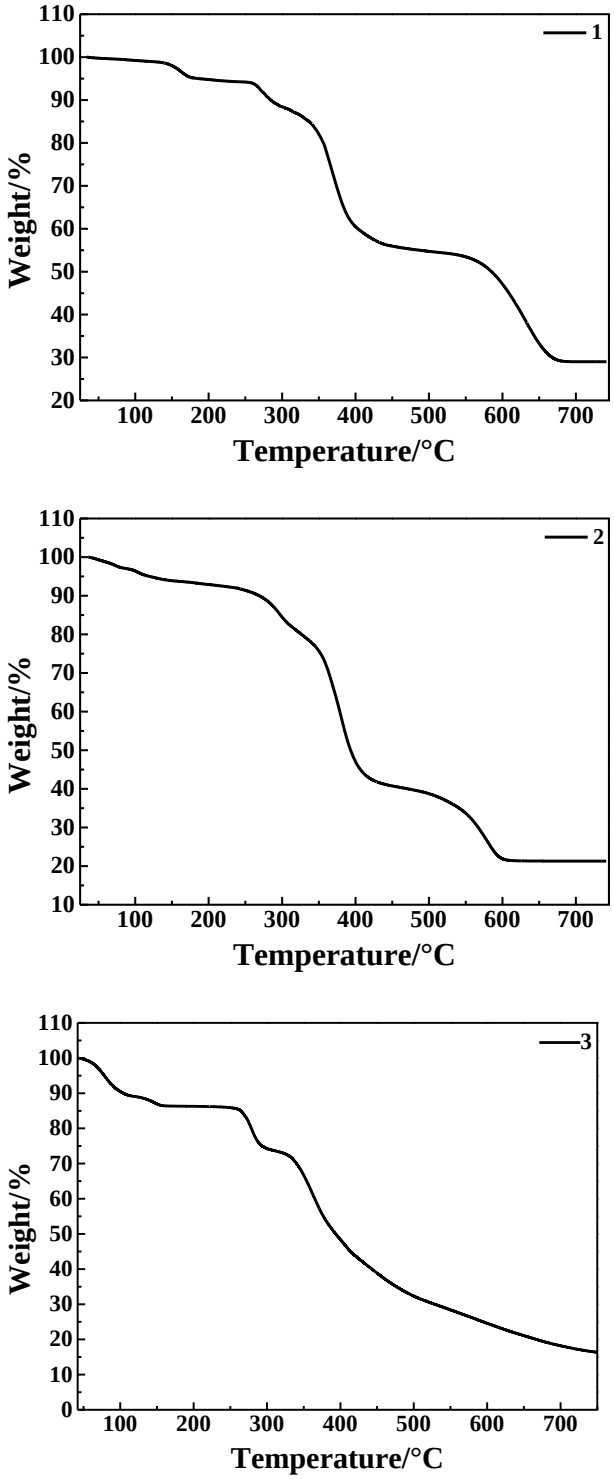

Figure S12. The TGA curves of **1–3**.

Section 4. Photophysical studies of 1–3

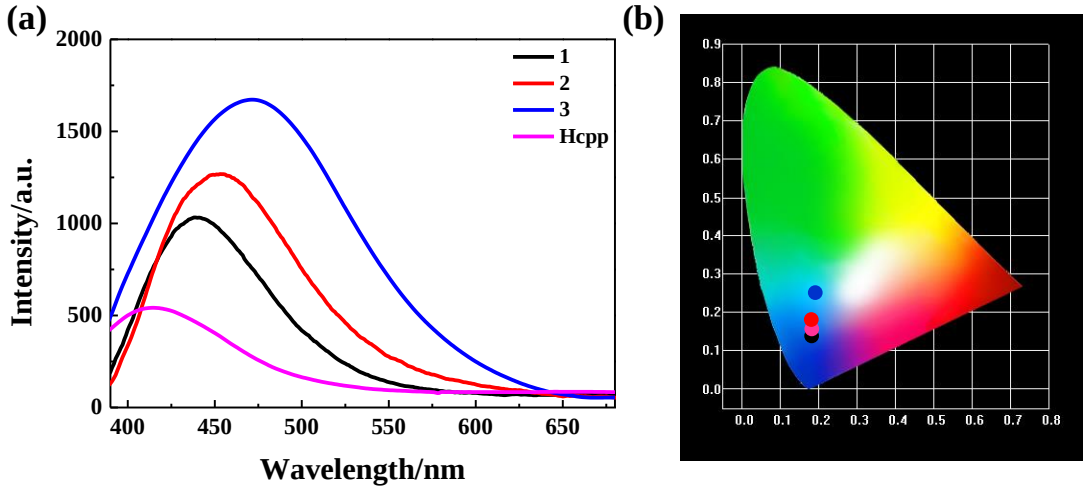

Figure S13. (a) Luminescent emission spectra of **1–3** and Hcpp at room temperature. (b) The CIE coordinates of **1–3** and Hcpp ligand under UV light.

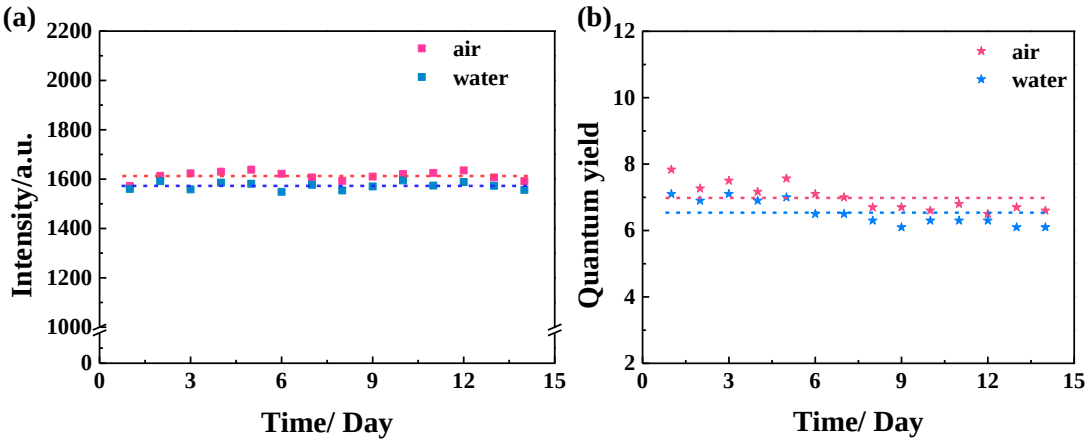

Figure S14. (a) Luminescent intensity of emission of **3** in placed air (pink square) and immersed in aqueous solution (blue square) for two weeks; (b) Quantum yield of emission of **3** placed in air (pink star) and immersed in aqueous solution (blue star) for two weeks.

Section 5. Solvent dependent dynamic property

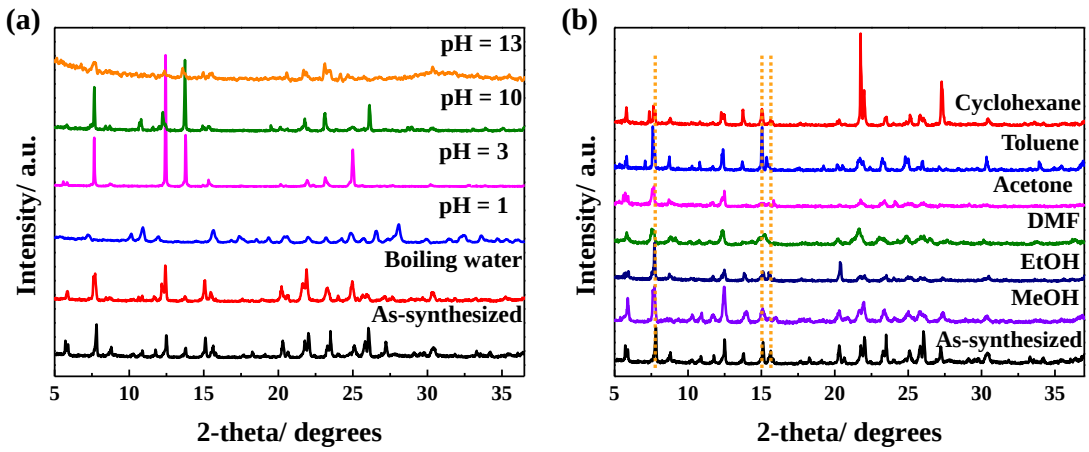

Figure S15. (a) PXRD patterns of **3** after being soaked in acidic and basic solutions; (b) PXRD patterns of **3** with different guest inclusion.

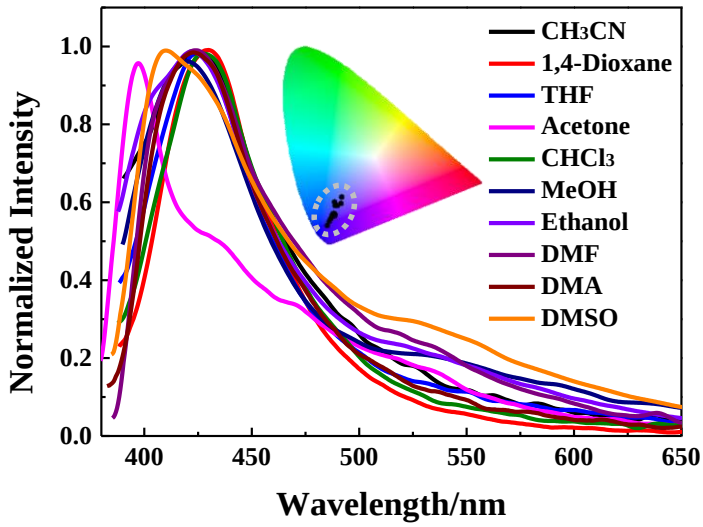

Figure S16. Normalized emissions of **3** in different solvents.

Table S6. Solvent dependent luminescence properties of **3**[a].

Solvent	Solvent parameters						Luminescent property		
	Reichardt's parameters		Kamlet-Taft parameters		Gutmann's parameters		λ_{max} (nm)	CIE X/ CIE Y	E_S (kcal mol^{-1})
	E_T^N	α	β	SPP	AN	DN			
Acetonitrile	0.460	0.19	0.40	0.66	18.9	14.1	425	(0.19,0.13)	67.13964
1,4-Dioxane	0.164	00	0.37	0.55	10.8	14.8	429	(0.17,0.08)	66.27598
THF	0.207	-	-	0.58	-	20	424	(0.19,0.13)	67.37852
Acetone	0.355	-	-	-	-	17	397	(0.19,0.18)	72.03258
Chloroform	0.259	-	-	0.49	-	00	428	(0.17,0.10)	66.74472
MeOH	0.762	0.98	0.66	0.60	41.5	19	419	(0.22,0.18)	68.1932
EtOH	0.654	0.86	0.75	0.54	37.9	19.2	421	(0.20,0.17)	67.62072
DMF	0.386	00	0.69	0.88	13.6	26.6	424	(0.19,0.17)	67.35231
DMA	0.377	00	0.76	0.85	16	27.8	422	(0.18,0.11)	67.45959
DMSO	0.444	00	0.76	1.00	19.3	29.8	410	(0.22,0.20)	70.05775

[a] λ_{max}: emission wavelength; E_S: singlet energy.

Section 6. DPA detection of Eu^{3+}@3 composite

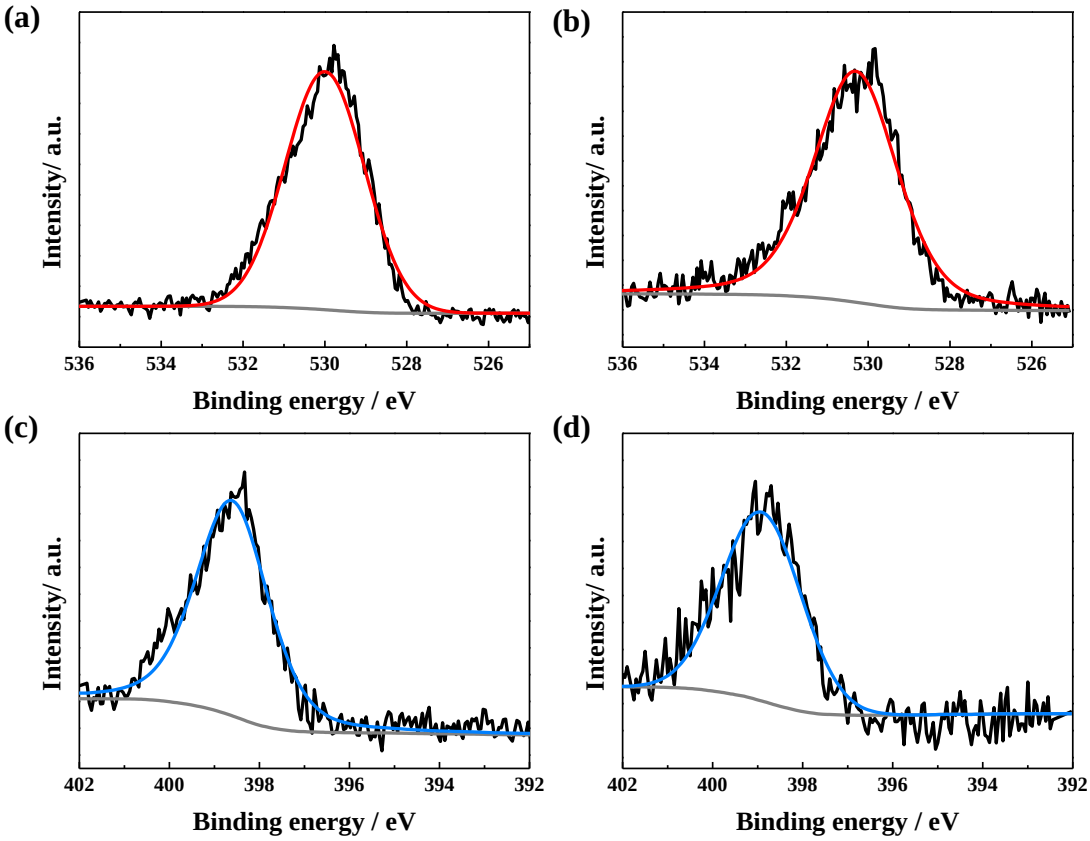

Figure S17. XPS spectra of O 1s peak for **3** (a) and Eu^{3+}@**3** (b); XPS spectra of N 1s peak for **3** (c) and Eu^{3+}@**3** (d).

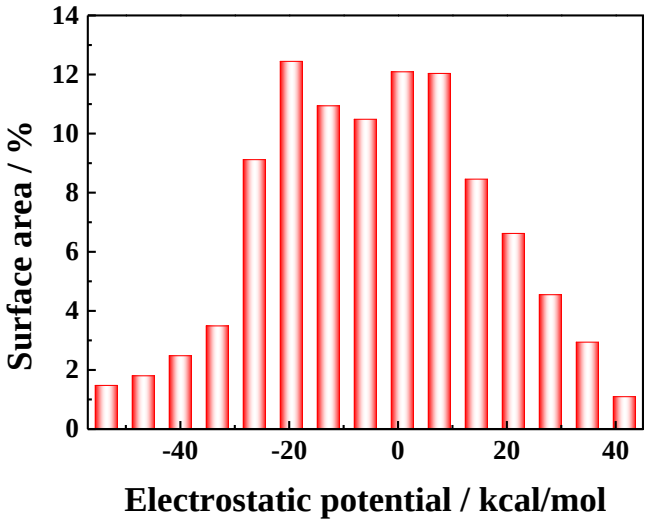

Figure S18. Surface area percent in each ESP range on the vdW surface.

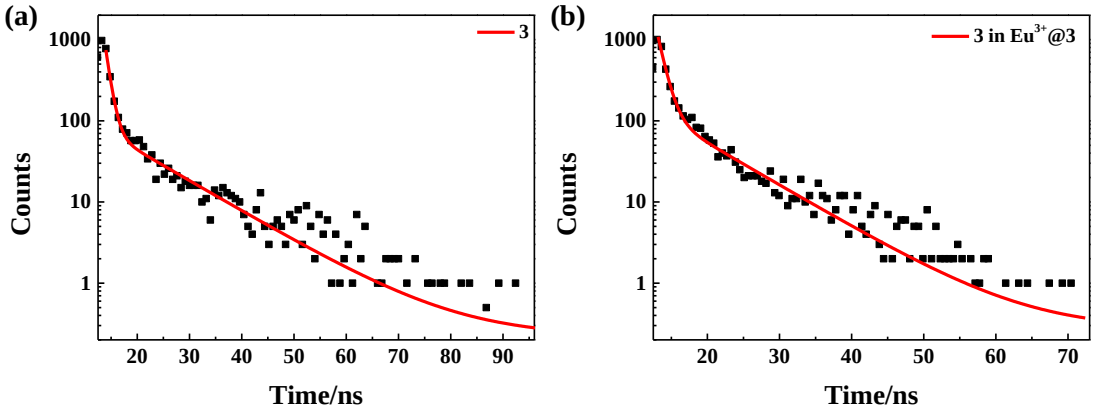

Figure S19. Luminescence decay curves of **3** before (a) and after (a) Eu^{3+} doping at 298 K.

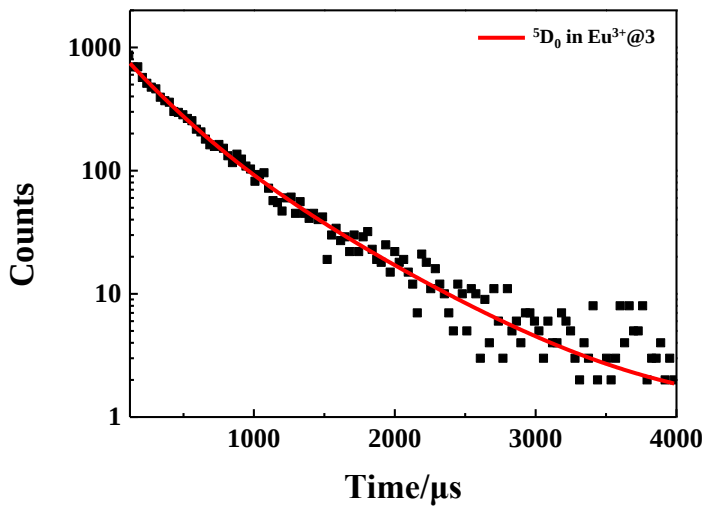

Figure S20. Luminescence decay curves of Eu^{3+} in Eu^{3+}@**3** at 298 K.

Table S7. RSD data of integrated intensity (I_{616}/I_{456}) after DPA addition.

Added DPA concentrations (μM)	Average value of I_{616}/I_{456}	RSD (n = 5) (%)
0	2.290	2.180
1.0	2.513	6.461
2.0	2.781	2.044
3.0	3.235	3.884
4.0	3.412	2.046
5.0	3.863	5.993
6.0	4.211	3.335
7.0	4.464	3.821

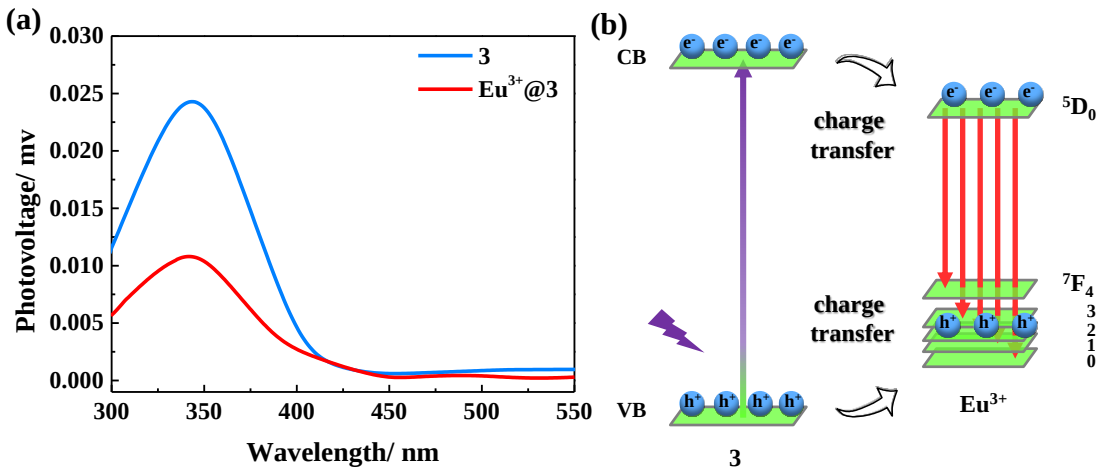

Figure S21. (a) Surface photovoltage spectroscopy (SPS) of **3** and Eu^{3+}@**3** samples; (b) Transfer and separation of photogenerated charges in Eu^{3+}@**3**.

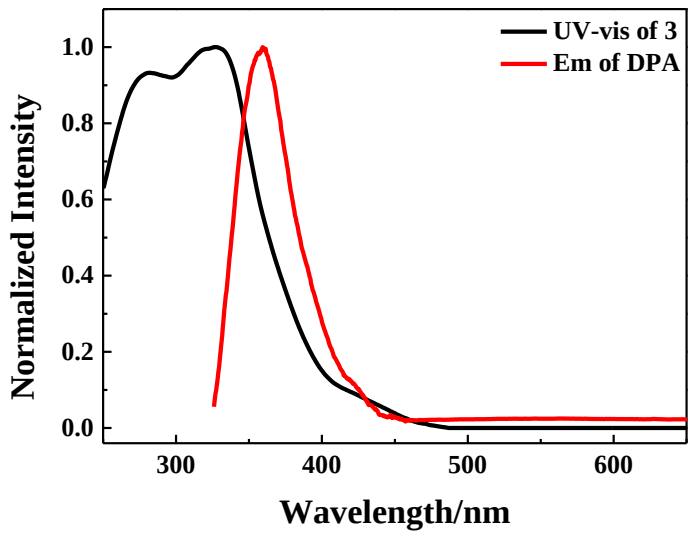

Figure S22. Spectral overlaps between normalized absorption spectra of **3** and the normalized emission spectra of DPA in water.

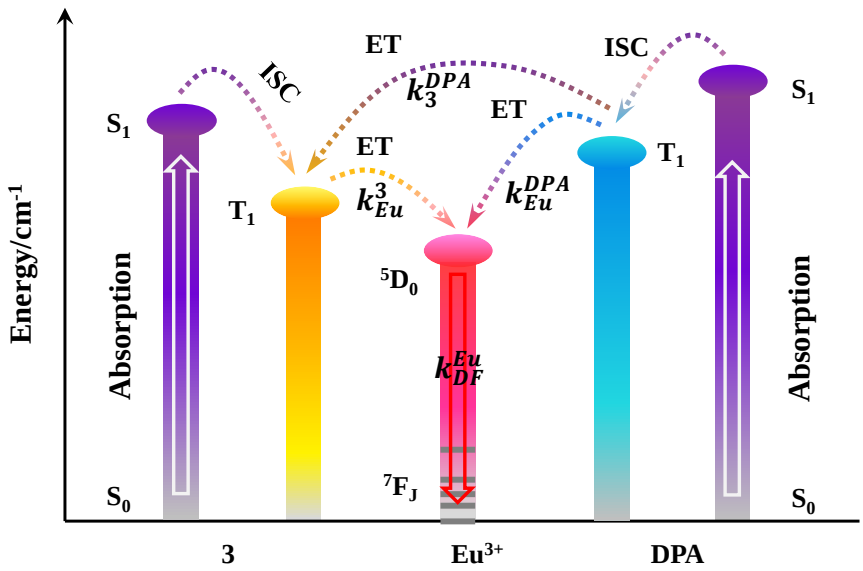

Figure S23. Schematic energy level diagrams and energy transfer mechanism of Eu^{3+}@**3** after addition of DPA. Abbreviations: S = singlet; T = triplet; ISC = intersystem crossing; ET = energy transfer; k = radiative or nonradiative transition probability.

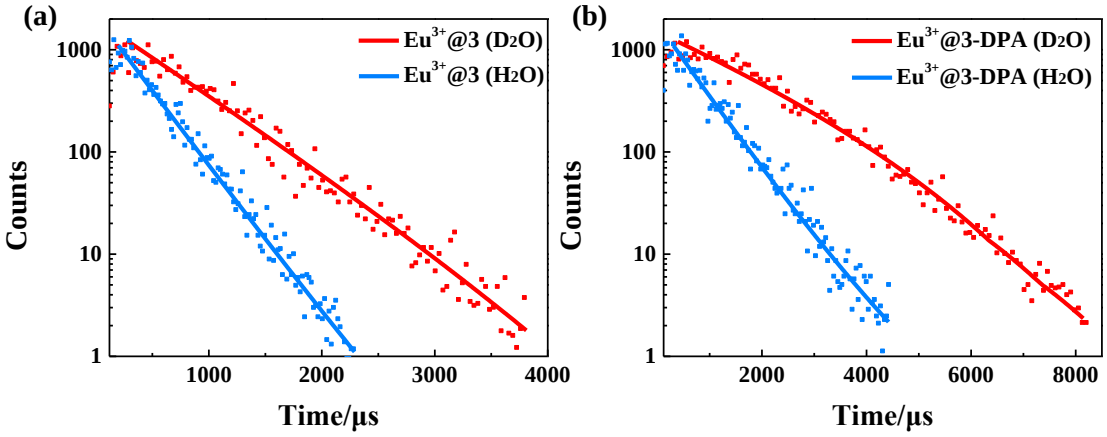

Figure S24. The luminescent decay curves of $^5D_0$ (Eu^{3+}) lifetimes of (a) Eu^{3+}@**3** and (b) Eu^{3+}@**3**-DPA (50 μM) in H_2O (blue) and D_2O (red).

Table S8. Luminescence lifetime τ and the number of water molecules coordinated to Eu^{3+}@**3** composite.

Sample	τ (μs)	K (μs^{-1})	q^a
Eu^{3+}@**3** (H_2O)	212.06	4.71	3.22
Eu^{3+}@**3** (D_2O)	562.12	1.78	
Eu^{3+}@**3** +DPA (50 μM) (H_2O)	732.49	1.36	0.34
Eu^{3+}@**3** +DPA (50 μM) (D_2O)	1224.97	0.82	

[a]*q* values were estimated according to the eq 1.

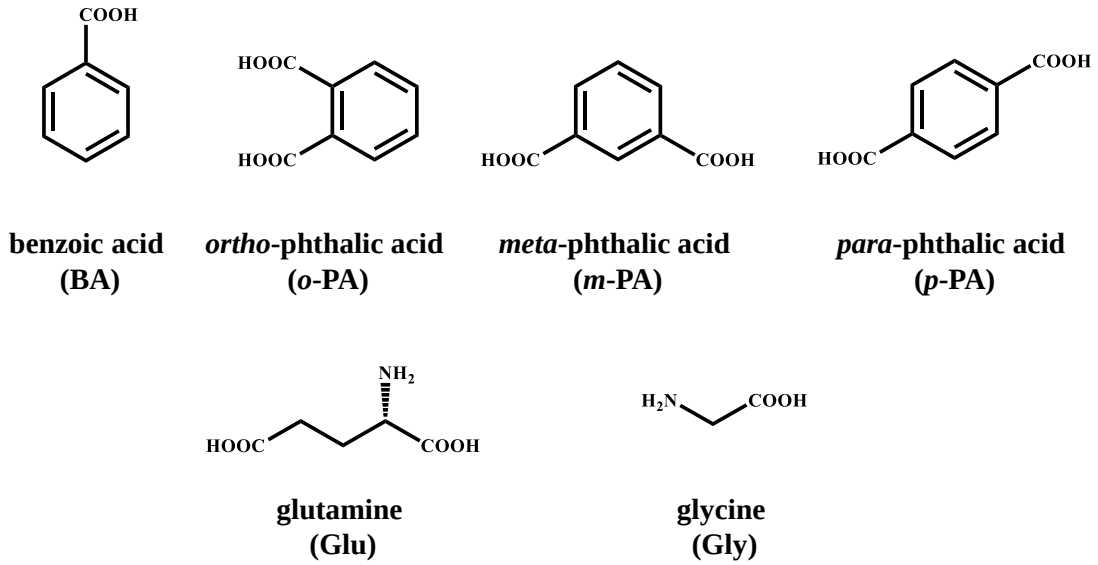

Figure S25. Molecular structures of the selected competition analytes.

Table S9. Determination of DPA in fetal calf serum samples for Eu^{3+}@**3**.

Added standard DPA (μM)	Founded DPA (μM)	RSD (n=5) (%)	Recovery (%)
1.00	1.06 ± 0.02	1.89	105.61
2.00	2.10 ± 0.01	0.48	105.10
3.00	2.96 ± 0.07	2.36	98.67

References

(1) Sheldrick, G. M. *SHELXL 97 Program for Crystal Structure Refinement*, University of Göttingen, Germany, 1997.

(2) Sheldrick, G. M. *SHELXL 97 Program for Crystal Structure Solution*, University of Göttingen, Germany, 1997.